First-Principles Full-Vectorial Eigenfrequency Computations for Axially Symmetric Resonators

Rohan D. Kekatpure

***Abstract*—Starting from the time-harmonic Maxwell's equations in cylindrical coordinates, we derive and solve the finite-difference (FD) eigenvalue equations for determining vector modes of axially symmetric resonator structures such as disks, rings, spheres and toroids. Contrary to the most existing implementations, our FD scheme is readily adapted for both eigen*mode* and eigen*frequency* calculations. An excellent match of the FD solutions with the analytically calculated mode indices of a microsphere resonator provides a numerical confirmation of the mode-solver accuracy. The comparison of the presented FD technique with the finite-element method highlights the relative strengths of both techniques and advances the FD mode-solver as an important tool for cylindrical resonator design.**

***Index Terms*—Eigenfrequency solver, finite difference method, finite element method, mode-solver, resonators, silicon photonics.**

I. Introduction

AXIALLY symmetric resonator structures (also known as cylindrically symmetric or cylindrical resonators) such as microdisks and microrings have played an increasingly prominent role in microphotonics research and development in the past two decades. Their simple fabrication and amenability to versatile testing procedures facilitates addition of complex optical functionality to cylindrical resonator devices. Consequently, they have been the backbone of on-chip active and passive components including filters [1], ultrafast all-optical switches [2], GHz-bandwidth modulators [3], and lasers [4]–[6]. Cylindrical resonator structures have also helped realize on-chip non-linear optical functionalities like comb-frequency generation [7] and four-wave mixing [8]. Due to their ability to provide ultrahigh quality-factors ($>10^9$) a majority of fundamental investigations of light-matter interaction are based on axially symmetric resonators like pedestal-supported microdisks [9]–[12], micro-toroids [13], and microsphere [14] resonators. More recently, high-Q microring resonators promise to bridge the disparate areas of nanophotonics and the nano-mechanics [15]. An effective utilization of cylindrical resonator structures for the above applications hinges on our ability to predict the optical performance (e.g., resonance wavelengths and quality factors) of the fabricated structures and to tailor the resonator geometry to obtain the desired performance. These tasks require an accurate knowledge of electromagnetic field distributions in these resonator structures.

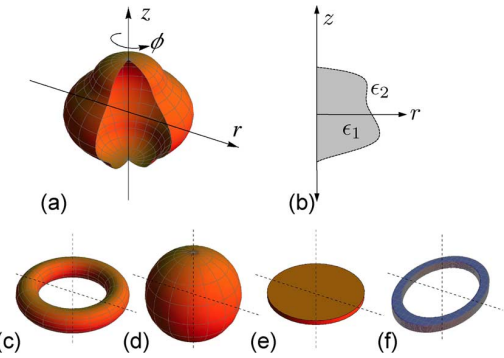

Fig. 1. (a) Schematic of a general cylindrically symmetric resonator structure. (b) rz cross section of the resonator structure used for finite-difference modeling. (c)–(f) Canonical axially symmetric resonator structures: micro-toroid (c), microsphere (d), microdisk (e), and microring (f).

Despite the rising importance of cylindrical resonators, a rigorous computational framework for their analysis is still not established as firmly as that for straight waveguides. Many commercial photonic design softwares lack cylindrical mode-solver capabilities and a few others have only recently begun to offer it [16], [17]. The details of implementation are often hidden in the commercial softwares and consequently it is difficult to interface them with other computational tools or customize them for particular design problems. As a result, a conceptually simple and a readily programmable technique for computing electromagnetic fields in axially symmetric structures is highly desired.

Any resonant structure possessing a rotational symmetry can, in principle, be classified as a cylindrical resonator (Fig. 1(a)). The majority of cylindrical resonators employed in practice, however, fall into four structural groups shown in Fig. 1(c)–(f). There have been a number of studies on the use of finite-difference (FD)-based discretization of time-harmonic Maxwell's equations for solution of cylindrical micro-resonator modes [18]–[20]. The main idea in a FD-based calculation is to assume a harmonic variation in the azimuthal ($\hat{\phi}$) direction to reduce the problem to two dimensions (r and z) as shown in Fig. 1(b).

Following the discretization of the r-z cross-section, most existing studies prescribe construction of a few matrices from the known material and geometric parameters of the problem and provide the manipulations of these matrices leading to the final eigenvalue equation to be solved using numerical routines

Manuscript received September 27, 2010; revised December 01, 2010; accepted December 02, 2010. Date of publication December 13, 2010; date of current version January 21, 2011. This work was supported by the Laboratory Directed Research and Development program at Sandia National Laboratories. Sandia is a multiprogram laboratory operated by Sandia Corporation, a Lockheed Martin Company, for the United States Department of Energys National Nuclear Security Administration under Contract DE-AC04-94AL85000.

The author is with Applied Photonics and Microsystems Division, Sandia National Laboratories, Albuquerque, NM 87123-3453 USA (e-mail: rdkekat@sandia.gov).

Color versions of one or more of the figures in this paper are available online at http://ieeexplore.ieee.org.

Digital Object Identifier 10.1109/JLT.2010.2099105

[20]. The matrices are obtained by mapping the native cylindrical coordinate system of the problem into an equivalent cartesian system using a local coordinate transformation [18]–[20]. With the exception of [21] most current approaches share the following common features: (1) They implement eigenmode solutions and do not distinguish between the eigen*mode* and eigen*frequency* variants of an eigenvalue solution. Whereas an eigenmode calculation is tailored to quantify waveguide bend losses, we argue that an eigenfrequency calculation is more naturally suited for cylindrical resonator designs. (2) Accuracy of the obtained mode indices is verified by confirming convergence with grid densification. Whereas this is a necessary condition for correct implementation, it does not provide an absolute measure of the accuracy (e.g., the mode indices may converge to wrong values). (3) A transformation from the native cylindrical to a local cartesian coordinate system is unnecessary for forming the eigenvalue equations—a set of cylindrical FD equations can be derived directly from time-harmonic Maxwell's equations. (4) Numerically, the specified manipulations result in denser eigenvalue equations (i.e., more non-zero elements in the sparse matrix) and consequently necessitate more time and computing resources for their solution. (5) Finally, from a general standpoint, the specified matrix manipulations make it difficult to understand and implement the algorithm. It is not readily deducible if the obtained eigenvectors obey the field transversality condition ($\nabla \cdot \mathbf{D} = 0$) which must be satisfied by any allowed mode.

In the present paper, we aim to demonstrate how the leaky eigenmodes of an arbitrary axially symmetric resonator may be calculated from first-principles without resorting to any local coordinate transformation. Starting directly from time-harmonic Maxwell's equations in a cylindrical coordinate system, we derive the master FD equation that can be readily adapted for either an eigenmode or an eigenfrequency calculation. The transversality condition is explicitly used in construction of this master equation and numerically it leads sparser system matrices. Most importantly, we provide a direct measure of the accuracy of calculations by comparing them against the analytically calculated modes of a microsphere resonator. The main factors distinguishing our work from the existing studies are a first-principles approach, lack of any coordinate transformations, and a rigorous error analysis of our implementation.

II. The Finite Difference Eigenvalue Equation

We start with time-harmonic Maxwell's equations with dependence $e^{i(\omega t - \mathbf{k}\cdot\mathbf{r})}$. For cylindrically symmetric resonators, the azimuthal dependence is assumed to be $e^{-i\nu\phi}$ where ν is an integer if the structure happens to be resonant at that wavelength. Using Chew's notation [22], we can express the time-harmonic Maxwell's equations as

$$\tilde{\nabla} \times \tilde{\mathbf{E}}_{\mathbf{m}} = -i\omega\mu_0 \hat{\mathbf{H}}_{\mathbf{m}+\frac{1}{2}} \tag{1}$$

$$\hat{\nabla} \times \hat{\mathbf{H}}_{\mathbf{m}+\frac{1}{2}} = i\omega\epsilon_0\epsilon_r(\mathbf{r})\tilde{\mathbf{E}}_{\mathbf{m}} \tag{2}$$

$$\hat{\nabla} \cdot \tilde{\mathbf{D}}_{\mathbf{m}} = 0 \tag{3}$$

$$\tilde{\nabla} \cdot \hat{\mathbf{H}}_{\mathbf{m}+\frac{1}{2}} = 0. \tag{4}$$

To obtain the eigenvalue equation, we first define the fields and the differential operators in a FD scheme

$$\tilde{\mathbf{E}}_{m,n} = \hat{r}E^r_{m+\frac{1}{2},n} + \hat{\phi}E^{\phi}_{m,n} + \hat{z}E^z_{m,n+\frac{1}{2}} \tag{5}$$

$$\hat{\mathbf{H}}_{m,n} = \hat{r}H_{m-\frac{1}{2},n} + \hat{\phi}H^{\phi}_{m+\frac{1}{2},n+\frac{1}{2}} + \hat{z}H_{m,n-\frac{1}{2}}. \tag{6}$$

The $\tilde{}$ and $\hat{}$ symbolize the forward and the backward differences respectively. Explicit expressions for $\tilde{\nabla}\times$, $\hat{\nabla}\times$, and $\hat{\nabla}\cdot$ can be found in [22]. The curl equations can be decomposed into their component form as follows. For the magnetic field we have:

$$H^r_{m,n+\frac{1}{2}} = \frac{-1}{i\omega\mu_0}\left(-\frac{i\nu}{r_m}E^z_{m,n+\frac{1}{2}} - \tilde{\partial}_z E^{\phi}_{m,n}\right) \tag{7a}$$

$$H^{\phi}_{m+\frac{1}{2},n+\frac{1}{2}} = \frac{-1}{i\omega\mu_0}\left(\tilde{\partial}_z E^r_{m+\frac{1}{2},n} - \tilde{\partial}_r E^z_{m,n+\frac{1}{2}}\right) \tag{7b}$$

$$H^z_{m+\frac{1}{2},n} = \frac{-1}{i\omega\mu_0}\left(\frac{1}{r_{m+\frac{1}{2}}}\tilde{\partial}_r r_m E^{\phi}_{m,n} + \frac{i\nu}{r_{m+\frac{1}{2}}}E^r_{m+\frac{1}{2},n}\right). \tag{7c}$$

Similarly the electric field equations can be expanded as:

$$i\omega\epsilon_{\mathbf{m}}E^r_{m+\frac{1}{2},n} = -\frac{i\nu}{r_{m+\frac{1}{2}}}H^z_{m+\frac{1}{2},n} - \hat{\partial}_z H^{\phi}_{m+\frac{1}{2},n+\frac{1}{2}} \tag{8a}$$

$$i\omega\epsilon_{\mathbf{m}}E^{\phi}_{m,n} = \hat{\partial}_z H^r_{m,n+\frac{1}{2}} - \hat{\partial}_r H^z_{m+\frac{1}{2},n} \tag{8b}$$

$$i\omega\epsilon_{\mathbf{m}}E^z_{m,n+\frac{1}{2}} = \frac{1}{r_m}\hat{\partial}_r r_{m+\frac{1}{2}}H^{\phi}_{m+\frac{1}{2},n+\frac{1}{2}} + \frac{i\nu}{r_m}H^r_{m,n+\frac{1}{2}}. \tag{8c}$$

We transform the six equations (7) and (8) into a two-component eigenvalue equation for $[E^r, E^z]^{\mathsf{T}}$ by eliminating $H^{r,z,\phi}$ and E^{ϕ} as shown in Appendix A to obtain the elemental finite-difference (FD) eigenvalue equation (9). The master equation derived here is analogous to the elemental FD equation stated in [21], shown in (9) at the bottom of the page.

III. Two Eigenvalue Types

Equation (9) is the master equation that can be cast and solved for two kinds of eigenvalues. In the first kind, one inputs the known operating frequency ω and solves the eigenvalue equation in the mode index ν. A majority of works in the literature [18]–[20] develop eigenvalue equations in terms of the mode-

$$\left(\begin{array}{c|c} -\hat{\partial}_z\tilde{\partial}_z - \frac{1}{r^2_{m+\frac{1}{2}}}\tilde{\partial}_r\frac{r_m}{\epsilon_{\mathbf{m}}}\hat{\partial}_r r_{m+\frac{1}{2}}\epsilon_{\mathbf{m}} & \hat{\partial}_z\tilde{\partial}_r - \frac{1}{r^2_{m+\frac{1}{2}}}\tilde{\partial}_r\frac{r^2_m}{\epsilon_{\mathbf{m}}}\hat{\partial}_z\epsilon_{\mathbf{m}} \\ \hline \frac{1}{r_m}\hat{\partial}_r r_{m+\frac{1}{2}}\tilde{\partial}_z - \frac{1}{r_m}\tilde{\partial}_z\frac{1}{\epsilon_{\mathbf{m}}}\hat{\partial}_r r_{m+\frac{1}{2}}\epsilon_{\mathbf{m}} & -\tilde{\partial}_z\frac{1}{\epsilon_{\mathbf{m}}}\hat{\partial}_z\epsilon_{\mathbf{m}} - \frac{1}{r_m}\hat{\partial}_r r_{m+\frac{1}{2}}\tilde{\partial}_r \end{array}\right)\left[\begin{array}{c} E^r_{m+\frac{1}{2},n} \\ E^z_{m,n+\frac{1}{2}} \end{array}\right]$$

$$= \left[\begin{array}{c|c} \omega^2\mu_0\epsilon_{\mathbf{m}} - \frac{\nu^2}{r^2_{m+\frac{1}{2}}} & 0 \\ \hline 0 & \omega^2\mu_0\epsilon_{\mathbf{m}} - \frac{\nu^2}{r^2_m} \end{array}\right]\left[\begin{array}{c} E^r_{m+\frac{1}{2},n} \\ E^z_{m,n+\frac{1}{2}} \end{array}\right] \tag{9}$$

index. This approach is the cylindrical analogue of the cartesian waveguide effective index determination procedure in which an effective index at a given wavelength (e.g., 1550 nm) is required. As mentioned in the introduction, cylindrical eigenmode calculations are suited for quantifying bend losses in waveguides.

The second kind of eigenvalue equation results when one inputs an integer mode-index ν and solves for the resonant frequency ω *around* the frequency of interest (e.g., corresponding to 1550 nm wavelength). This class of eigenvalue solution is more naturally suited for the design of cylindrically symmetric resonators because the resonant frequency and the quality factor are anchored to the structure geometry (e.g., radius, thickness). In other words, using passive means alone, one usually cannot *independently* fix the resonator dimensions *and* its resonance frequencies. In most design situations, the resonator dimensions are subject to material and performance constraints. For instance, in the field of silicon photonics which employs cylindrical resonators in abundance [1]–[3], [23], the thickness is determined by the wafer-scale silicon-on-insulator (SOI) layer thickness while the in-plane dimensions are constrained by the electrical metrics such as the RC time constants and the power consumption. In such situations, an eigenfrequency solution determines the resonance frequencies for given geometry and mode order ν.

The master equation (9) however, is readily adopted to solve both types of eigenvalue problems by a simple re-arrangement of right-hand side terms. Due to the prevalence of eigenmode formulations in the literature, we illustrate our procedure using the eigenfrequency formulation.

IV. Leaky Eigenvalue Solutions Using Perfectly Matched Layers

Because of finite bending radius, the whispering gallery modes (WGMs) of cylindrical resonators experience propagation loss even if the core/cladding materials are lossless. Even for resonators with large radii and high refractive index contrasts (e.g., in a silicon/SiO_2 system), there usually exists a negligible but finite bending loss that must be captured in an eigenvalue calculation. To approximate such 'open' resonator systems, the energy escaping the resonator needs to be irreversibly absorbed to prevent it from being (numerically) reflected from the simulation domain walls back to the resonator. Such a reflection-less termination is effected in a calculation by padding the simulation domain with perfectly matched layers (PMLs) that absorb the leaked energy. Among the equivalent formulations of the PML's [24], [25] we adopt the one based on the complex-coordinate stretching. As per the prescription of this formulation, the coordinate ζ (representing either r or z) in which the absorption is desired is 'stretched' in the PML domain according to a stretching factor $s_\zeta(\zeta)$ given by

$$d\tilde{\zeta} = s_\zeta(\zeta)d\zeta. \tag{10}$$

For minimizing reflections, the stretching factor s_ζ is assigned a non-linear dependence on the coordinate ζ according to a polynomial relationship

$$s_\zeta = \begin{cases} 1 - \frac{i\sigma_{\max}}{\omega\epsilon_0}\left(\frac{|\zeta-\zeta_0|}{d_\zeta}\right)^p, & \text{in PML regions} \\ 1, & \text{otherwise} \end{cases} \tag{11}$$

TABLE I
Values of Material and Geometric Parameters for Finite Difference Calculation of Microdisk Eigenfrequencies

Parameter	Value
Si refractive index	3.5
SiO_2 refractive index	1.45
Microdisk radius	2 μm
Microdisk thickness	250 nm
Radial grid density	25 nm
Axial grid density	25 nm
Mode number ν	19
PML thicknesses	1 μm

where ζ_0 is the starting location of the PML, d_ζ is the PML thickness normal to the ζ-coordinate and $p = 2$ is typically used to obtain a parabolic stretching. For the usually encountered case of piecewise constant permittivity, the Helmholtz operator expressed in cartesian coordinates does not depend on x, y, or z coordinates. Hence, the integrated form of (10) to obtain $\tilde{\zeta}(\zeta)$ explicitly is unnecessary. The cylindrical Helmholtz operator equation (9), however, depends explicitly on the radial co-ordinate r. It is therefore necessary to integrate (10) obtain the stretched radial coordinate $\tilde{r}$ according to

$$\tilde{r} = \begin{cases} r - \frac{i\sigma_{\max}}{(p+1)\omega\epsilon_0}\left(\frac{|r-r_0|}{d_r}\right)^{p+1}, & \text{in PML regions} \\ r, & \text{otherwise.} \end{cases} \tag{12}$$

Like the cartesian PMLs, the grid spacings, of course, also need to be scaled as $\Delta\tilde{r} \to s_r(r)\Delta r$ and $\Delta\tilde{z} \to s_z(z)\Delta z$ in the PML regions of the simulation domain. The PML thickness is determined by starting from any reasonable value (e.g., half wavelength) and increasing it gradually till the obtained mode indices are uninfluenced by the increasing PML thickness.

Mathematically, a PML truncation of the simulation domain introduces complex values in the Helmholtz operator matrix and forces the eigenvalue solver to search for the complex eigenfrequencies $\omega_{\mathrm{R}} + i\omega_{\mathrm{I}}$. Physically, the imaginary part of the complex eigenfrequency signifies dissipation of the resonator energy with time and represents loss. In the absence of material loss, the approximate value of the radiation Q can be computed from the imaginary eigenfrequency as $Q = \omega_{\mathrm{R}}/(2\omega_{\mathrm{I}})$.

V. Example Results for a Microdisk Resonator

We illustrate the working of our cylindrical mode-solver by calculating the resonant modes around 1550 nm wavelength of a silicon microdisk resonator clad by silicon dioxide. This type of resonator structure has been employed abundantly in designs of various integrated nanophotonic structures such as modulators, switches, and filters. The material and geometric parameters used in this simulation are recorded in Table I. The values for thickness are based on the typical Si device layer thickness used in SOI-based photonic structures. The radius of 2 μm ensures an observable amount of radiation leakage and helps test the working of the PML implementation.

Using parameter values in Table I, (9) resulted in an eigenvalue matrix with 1613352 non-zero elements. We computed the eigenvalues and the eigenvectors of this matrix using the MATLAB™ `eigs` subroutine and obtained a complex resonance wavelength of $1546.591 - i1.0992 \times 10^{-4}$ nm corresponding to a radiation Q of 7.035×10^6. On our computer (Intel™ Xeon

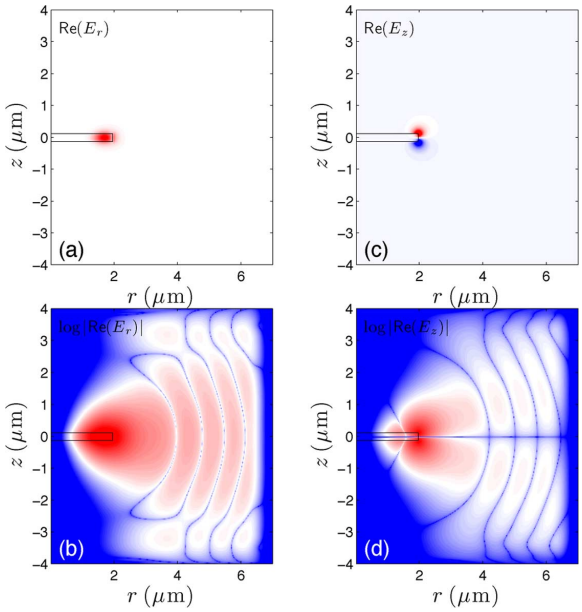

Fig. 2. Real parts of the electric fields of the fundamental mode of a 2 μm radius and 250 nm thick SiO_2-clad silicon microdisk (see Table I). (a) $\mathrm{Re}(E_r)$ and (c) $\mathrm{Re}(E_z)$ on a linear scale illustrating the field profiles of the radial and the axial electric fields. Same plots on the logarithmic scale (b) $\log|\mathrm{Re}(E_r)|$ and (d) $\log|\mathrm{Re}(E_r)|$ illustrating the radiation leakage and its absorption by the PMLs.

dual quad core processor with 10 GB memory running Macintosh™ OS-X) we recorded a peak memory usage of 2.0 GB and a solution time of 149 s. Solving the same problem as an eigen*mode* problem using direct matrix manipulations [20] resulted in an eigenvalue matrix with 3433330 non-zero elements, used 4.0 GB peak memory and took 180 s to solve.

VI. Error Analysis of FD Mode-Solver

It is usually difficult to quantify the numerical accuracy of the FD calculations using analytical means. Conventionally therefore, the accuracy of mode-solver solutions is confirmed by verifying convergence of eigenvalues with decreasing mesh size or by comparisons with benchmark structures. Although a satisfaction of these conditions is necessary for inferring the accuracy, they are insufficient as absolute indicators of convergence to the correct values. As such, we verify our implementation by comparing the complex eigenfrequencies of a microsphere resonator whose modes are amenable to an analytical solution.

For high azimuthal mode numbers (ν), a microsphere resonator admits predominantly TE or TM modes that can be determined analytically without resorting to the effective index method [26]. In the past decade, microsphere resonators have been studied in detail in the context of atomic physics [4], [13], [14] and their modal structure is well understood. Here we state the form of the modal solutions and the dispersion equation that determines the complex eigenfrequencies. With reference to spherical co-ordinate system depicted in Fig. 3, the only non-zero fields for TE/TM modes of a microsphere are (H^ϕ, E^r, E^θ) for a TE mode and (E^ϕ, H^r, H^θ) for a TM mode. The transverse (r and θ) components can be eliminated in both these cases to form a *scalar* equation in terms of the ϕ

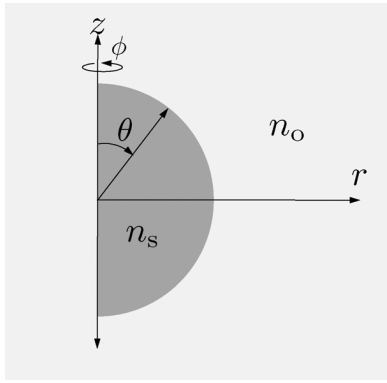

Fig. 3. Representation of the microsphere geometry in spherical and cylindrical coordinate system.

component. The solution of this equation yields the field profile as

$$F^\phi(r,\theta,\phi) = \begin{cases} Aj_\ell(kn_\mathrm{s}r)Y_\ell^\nu(\theta,\phi) & r < a \\ Bh_\ell^{(1)}(kn_\mathrm{o}r)Y_\ell^\nu(\theta,\phi) & r \geq a \end{cases} \tag{13}$$

where j_ℓ and $h_\ell^{(1)}$ are, respectively, the spherical Bessel function and Hankel function of the first kind of order ℓ and Y_ℓ^ν is the spherical harmonic of degree ℓ and order ν. F^ϕ represents either the azimuthal field H^ϕ for a TE mode or E^ϕ for a TM mode. Enforcing continuity of the tangential fields at $r = a$ yields the transcendental dispersion equation determining the resonant frequencies and Q's of the allowed modes:

$$\frac{j_\ell'(kn_\mathrm{s}a)}{j_\ell(kn_\mathrm{s}a)} = q\frac{h_\ell'(kn_\mathrm{o}a)}{h_\ell(kn_\mathrm{o}a)} \tag{14}$$

where the polarization factor $q = {n_\mathrm{s}}^2/{n_\mathrm{o}}^2$ for a TE mode and $q = 1$ for a TM mode. The spherical Hankel function is a complex superposition of the spherical Bessel functions of the first and the second kinds: $h_\ell^{(1)}(z) \equiv j_\ell(z) + iy_\ell(z)$. As a result, the dispersion (14) possesses solutions with complex $k : k = k_\mathrm{R} + ik_\mathrm{I}$. The imaginary part of k signifies the radiation loss and yields the radiation $Q = k_\mathrm{R}/(2k_\mathrm{I})$.

Despite its simple form, (14) is exceedingly difficult to solve for high-index-contrast spherical resonators. This is due to the fact that for high-Q modes ($Q > 10^{13}$), k_R and k_I can differ by several orders of magnitude ($>10^{13}$) making the numerical routines experience instabilities. It is also difficult to provide a complex initial guess that is required for a numerical solution of transcendental equations. We used the numerical package MATHEMATICA™ for a direct solution of (14). The roots were searched in an iterative fashion by using the preceding complex solution as the initial guess for the next iteration. The solutions usually converged after 4–5 iterations.

To benchmark the performance of our mode-solver we chose a 2 μm radius silicon ($n_\mathrm{s} = 3.5$) microsphere surrounded uniformly by silicon dioxide ($n_\mathrm{o} = 1.45$). Following an analytical calculation of the complex eigenfrequencies, we used our cylindrical FD mode-solver for a numerical calculation of the eigenfrequencies by treating the microsphere as an *axially* symmetric system. All calculations were performed using a uniform grid spacing of $\Delta r = \Delta z = 25$ nm. To eliminate the singularities on the z axis, the simulation domain began 1 grid point (25

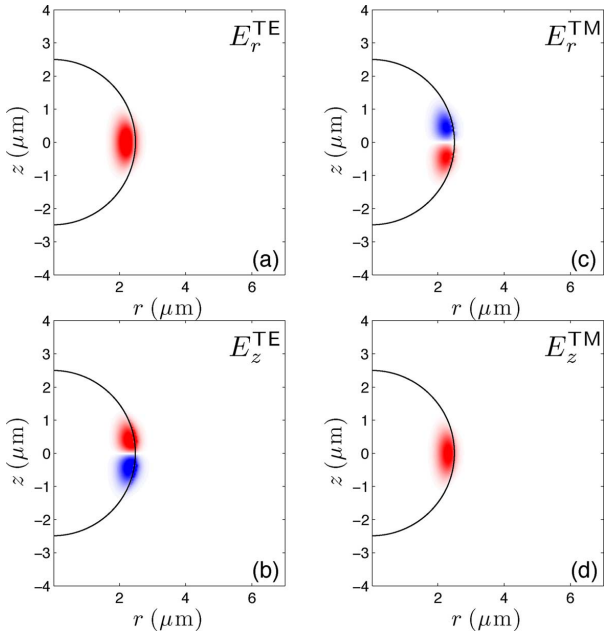

Fig. 4. Real parts of the electric fields of the fundamental mode of an SiO_2-clad 2 μm radius silicon microsphere. (a) $\mathrm{Re}(E_r)$ and (b) $\mathrm{Re}(E_z)$ of a TE mode. (c) $\mathrm{Re}(E_r)$ and (d) $\mathrm{Re}(E_z)$ of a TM mode.

nm) to the right of $r = 0$ boundary. All the boundaries were terminated with perfect electrically conducting (PEC) walls. The E^r and E^z fields of the TE and the TM modes obtained using the mode-solver are depicted in Fig. 4.

The comparison with analytical solutions was carried out in two ways. First, the analytical and FD calculations were performed for the 2 μm radius microsphere for different azimuthal mode numbers (ν). For increasing values of ν, this calculation provides successive resonance wavelengths. Figs. 5(a) and (c) show the comparison of the analytical and the FD solution for TE and TM modes. As seen from the plots, we obtain excellent agreement of the mode-solver results with the analytical calculations. The maximum fractional difference between analytical and FD calculations is $<0.35\%$ for TE modes and $<0.1\%$ for the TM modes over the entire wavelength considered. The free spectral range (FSR) is defined as the difference between successive resonance frequencies (or wavelengths) of a resonator and is an important design parameter. For the TE mode, the FSRs of the above microsphere resonator around 1550 nm predicted by the analytical and the FD calculations are 45.38 nm and 45.56 nm respectively. Similarly, for the TM mode, the corresponding values are 47.90 (analytical) nm and 47.92 nm (FD). The quality factors for the TE and the TM modes shown in Fig. 5(b) and (d) display an equally good agreement. For example, for the TE resonance mode at 1555.6 nm, the quality factors evaluated using analytical and the FD methods are, respectively, 4.10×10^{13} and 4.14×10^{13}. For the TM mode at 1599.0 nm the Q's are 4.12×10^{13} (analytical) and 4.52×10^{13} (FD).

Despite the close match, there is a finite numerical disagreement in the resonance wavelengths, FSRs and Qs calculated by the FD and analytical techniques. This difference could be caused by several factors such as: (1) dependence of analytical

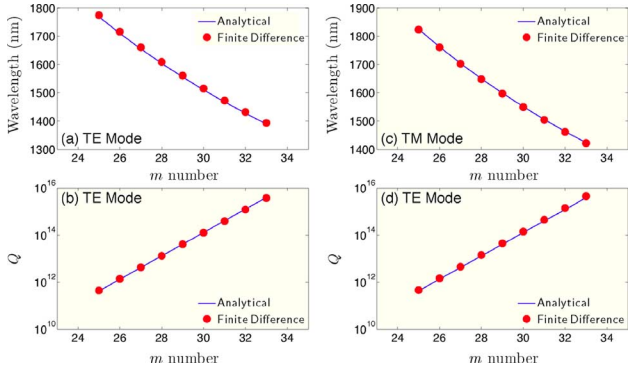

Fig. 5. Comparison of the resonance wavelengths and quality factors calculated using analytical (solid blue lines) and finite difference (red discs) techniques. (a) and (b) are resonance wavelengths and quality factor respectively, for the TE mode and (c) and (d) are the corresponding quantities for the TM mode.

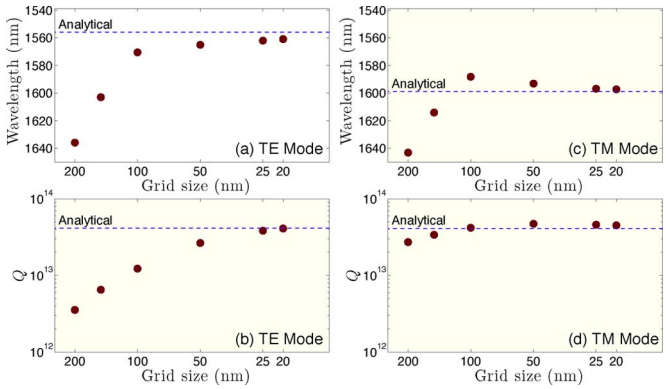

Fig. 6. Variation of the resonance wavelengths and the quality factors with decreasing mesh size for the TE mode [(a) and (b)] and the TM mode [(c) and (d)].

and FD calculations on initial guess, (2) scalar approximation made in analytical calculation, and (3) mesh discretization. The dependence of the complex eigenvalue on the initial guess for high-Q modes could be improved in an iterative fashion. Following this technique, we carry out the calculations a few times by using the the preceding solution as the initial guess for the current calculation and usually obtaining convergence within 4–5 steps. In our experience, the iteration needs to be carried out for *both* analytical and FD techniques when investigating the high-Q modes $(Q > 10^{14})$. To investigate the behavior of the resonance wavelengths and Qs with varying grid size, we solved for the TE and TM modes of the same microsphere considered above by varying the grid size between 200 nm and 20 nm (minimum allowed by our computing resource). The values of the grid sizes were chosen such that the microsphere radius spans an integer number of grid points. Figs. 6 shows how the resonance wavelength and the quality factor of the TE mode approach the analytical value with finer mesh sizes.

The approach of the FD calculations to the analytical values points to the discretization error as one of the primary factors responsible for the slight numerical disagreement between the analytical and the FD results for a 25 nm grid size. The converging trend in Fig. 6, however, indicates that closer agreements may be possible with denser meshes.

TABLE II
COMPARISON OF RESONANCE FREQUENCIES AND QUALITY FACTORS CALCULATED USING FD- AND FEM-BASED AXIAL MODE-SOLVERS

Quantity	Analytical	FD	FEM
$\lambda_{\rm res}$ (TE)	1484.93 nm	1489.0 nm	1486.30 nm
$\lambda_{\rm res}$ (TM)	1531.69 nm	1531.96 nm	1531.69 nm
$Q_{\rm TE}$	3.56×10^4	3.00×10^4	3.37×10^4
$Q_{\rm TM}$	5.18×10^4	5.46×10^4	5.15×10^4
Peak memory usage	-	2.20 GB	4.35 GB
Solution time	-	83 s	400 s

VII. COMPARISON WITH THE FINITE ELEMENT METHOD

The finite element method (FEM) is another well-established numerical technique for solution of electromagnetic boundary- and eigenvalue problems [27]. Unlike FD method which discretizes the *differential equation*, FEM assumes a polynomial form (with unknown coefficients) for the *solution* on the discretized geometry. The degree of the assumed polynomial is termed the 'element order.' FEM makes it straightforward to discretize curved geometries using non-uniform and non-rectangular meshing. This increased accuracy comes, of course, at the cost of a substantially increased programming effort. There exist numerous stable and user-friendly commercial electromagnetic FEM packages that eliminate most of the programming effort in FEM [16], [17], [28].

FEM-based axial mode-solvers have been employed for analyses of various resonator systems [4]–[6], [9]–[12]. A detailed report of an FEM axial mode-solver based on COMSOL MULTIPHYSICS [28] has been provided by Oxborrow [29]. To compare between FD and FEM with regard to their accuracy and resource usage, we developed a FEM-based axial mode-solver following [29]. Furthermore, for a fair comparison, we augmented Oxborrow's implementation by effecting cylindrical PMLs in the FEM. As a benchmark problem, we chose to compute modes of an SiO_2-clad, 5 μm-diameter microsphere resonator made of a polymeric material of relative permittivity 2.5. This value of permittivity results in Q's in 10^4–10^5 range and helps test the working of PMLs for FD and FEM mode-solvers. As before, the exact resonance frequencies and Q's were calculated using analytical method described in Section VI. Table II shows the mode indices and quality factors calculated using the three techniques.

From Table II it can be deduced that FEM is slightly more accurate than FD at predicting the quality factors and resonance wavelengths of the microsphere. This is consistent with our previous conclusion of geometry discretization being the primary source of error in FD calculations and FEM's superiority over FD at meshing curved geometries.

VIII. SUMMARY

We have presented a first-principles calculation of leaky resonant modes of axially symmetric resonators free of any local coordinate transformation. The derived master FD equation is readily adapted for either an eigenfrequency or an eigenmode analysis. A rigorous error analysis of our mode-solver implementation was carried out by comparing the FD-calculated complex resonance eigenfrequencies of a microsphere resonator with analytically determined values. Over the entire parameter range considered, we obtained a better than 0.35% accuracy in complex eigenfrequencies for the TE and TM modes. Convergence of the FD calculations to analytical values with increasing grid density identifies the discretization error as the primary contributor to the residual numerical disagreement between the FD and analytical calculations. Overall, the presented first-principles approach is easy to implement and a valuable tool for design of axially symmetric resonator structures.

APPENDIX A
DERIVATION OF THE MASTER EIGENVALUE EQUATION

First substitute $H^{\phi}_{m+1/2,n+1/2}$ $H^{z}_{m+1/2,n}$ from (7a) into (8a) to obtain

$$\begin{aligned} i\omega\epsilon_{\mathbf{m}}E^{r}_{m+\frac{1}{2},n} = &-\frac{i\nu}{r_{m+\frac{1}{2}}}\left(\frac{-1}{i\omega\mu_0}\right)\left(\frac{1}{r_{m+\frac{1}{2}}}\tilde{\partial}_r r_m E^{\phi}_{m,n}\right. \\ &\left.+\frac{i\nu}{r_{m+\frac{1}{2}}}E^{r}_{m+\frac{1}{2},n}\right) \\ &-\hat{\partial}_z\left(\frac{-1}{i\omega\mu_0}\right)\left(\tilde{\partial}_z E^{r}_{m+\frac{1}{2},n}-\tilde{\partial}_r E^{z}_{m,n+\frac{1}{2}}\right). \end{aligned}$$

Hence

$$\begin{aligned} \omega^2\mu_0\epsilon_{\mathbf{m}}E^{r}_{m+\frac{1}{2},n} = &-\frac{i\nu}{r^2_{m+\frac{1}{2}}}\tilde{\partial}_r r_m E^{\phi}_{m,n} \\ &+\frac{\nu^2}{r^2_{m+\frac{1}{2}}}E^{r}_{m+\frac{1}{2},n} \\ &-\hat{\partial}_z\tilde{\partial}_z E^{r}_{m+\frac{1}{2},n}+\hat{\partial}_z\tilde{\partial}_r E^{z}_{m,n+\frac{1}{2}} \end{aligned}$$

which implies

$$\begin{aligned} \left(\omega^2\mu_0\epsilon_{\mathbf{m}}-\frac{\nu^2}{r^2_{m+\frac{1}{2}}}\right)E^{r}_{m+\frac{1}{2},n} = &-\hat{\partial}_z\tilde{\partial}_z E^{r}_{m+\frac{1}{2},n} \\ &+\hat{\partial}_z\tilde{\partial}_r E^{z}_{m,n+\frac{1}{2}}-\frac{i\nu}{r^2_{m+\frac{1}{2}}}\tilde{\partial}_r r_m E^{\phi}_{m,n}. \end{aligned} \quad (15)$$

Similarly, substitute $H^{r}_{m,n+1/2}$ and $H^{\phi}_{m+1/2,n+1/2}$ from (7b) into (8c) to obtain

$$\begin{aligned} i\omega\epsilon_{\mathbf{m}}E^{z}_{m,n+\frac{1}{2}} = &\frac{1}{r_m}\hat{\partial}_r r_{m+\frac{1}{2}} \\ &\times\left(\frac{-1}{i\omega\mu_0}\right)\left(\tilde{\partial}_z E^{r}_{m+\frac{1}{2},n}-\tilde{\partial}_r E^{z}_{m,n+\frac{1}{2}}\right) \\ &+\frac{i\nu}{r_m}\left(\frac{-1}{i\omega\mu_0}\right)\left(\frac{-i\nu}{r_m}E^{z}_{m,n+\frac{1}{2}}-\tilde{\partial}_z E^{\phi}_{m,n}\right) \end{aligned}$$

Hence

$$\begin{aligned} \omega^2\mu_0\epsilon_{\mathbf{m}}E^{z}_{m,n+\frac{1}{2}} = &\frac{1}{r_m}\hat{\partial}_r r_{m+\frac{1}{2}}\tilde{\partial}_z E^{r}_{m+\frac{1}{2},n} \\ &-\frac{1}{r_{m+\frac{1}{2}}}\hat{\partial}_r r_m\tilde{\partial}_r E^{z}_{m,n+\frac{1}{2}} \\ &+\frac{\nu^2}{r^2_m}E^{z}_{m,n+\frac{1}{2}}-\frac{i\nu}{r_m}\tilde{\partial}_z E^{\phi}_{m,n}, \end{aligned}$$

which implies

$$\left(\omega^2\mu_0\epsilon_{\mathbf{m}} - \frac{\nu^2}{r_m^2}\right) E^z_{m,n+\frac{1}{2}} = \frac{1}{r_m}\hat{\partial}_r r_{m+\frac{1}{2}}\tilde{\partial}_z E^r_{m+\frac{1}{2},n} - \frac{1}{r_m}\hat{\partial}_r r_{m+\frac{1}{2}}\tilde{\partial}_r E^z_{m,n+\frac{1}{2}} - \frac{i\nu}{r_m}\tilde{\partial}_z E^\phi_{m,n} \quad (16)$$

Determination of $E^\phi_{m,n}$: Determination of $E^\phi_{m,n}$ requires use of Gauss's law (3)

$$\hat{\nabla}\cdot\tilde{\mathbf{D}}_{\mathbf{m}} = \hat{\nabla}\cdot(\epsilon_{\mathbf{m}}\tilde{\mathbf{E}}_{\mathbf{m}}) = 0,$$

which can be expanded as

$$\frac{1}{r_m}\hat{\partial}_r r_{m+\frac{1}{2}}\epsilon_{\mathbf{m}}E^r_{m+\frac{1}{2},n} - \frac{i\nu}{r_m}\epsilon_{\mathbf{m}}E^\phi_{m,n} + \hat{\partial}_z\epsilon_{\mathbf{m}}E^z_{m,n+\frac{1}{2}}$$

giving $E^\phi_{m,n}$ as

$$E^\phi_{m,n} = \frac{r_m}{i\nu\epsilon_{\mathbf{m}}}\left(\frac{1}{r_m}\hat{\partial}_r r_{m+\frac{1}{2}}\epsilon_{\mathbf{m}}E^r_{m+\frac{1}{2},n} + \hat{\partial}_z\epsilon_{\mathbf{m}}E^z_{m,n+\frac{1}{2}}\right)$$

The final elemental FD equation, (9), is obtained by substituting the above expression for $E^\phi_{m,n}$ into (15) and (16).

ACKNOWLEDGMENT

The author thanks Dr. F. B. McCormick and C. A. Boye for their support and encouragement.

REFERENCES

[1] B. Little, S. Chu, H. Haus, J. Foresi, and J.-P. Laine, "Microring resonator channel dropping filters," *J. Lightw. Technol.*, vol. 15, no. 6, pp. 998–1005, 1997.

[2] V. R. Almeida, C. A. Barrios, R. R. Panepucci, and M. Lipson, "All-optical control of light on a silicon chip," *Nature*, vol. 431, no. 7012, pp. 1081–1084, 2004.

[3] Q. Xu, B. Schmidt, S. Pradhan, and M. Lipson, "Micrometre-scale silicon electro-optic modulator," *Nature*, vol. 435, no. 7040, pp. 325–327, 2005.

[4] T. J. Kippenberg, J. Kalkman, A. Polman, and K. J. Vahala, "Demonstration of an erbium-doped microdisk laser on a silicon chip," *Phys. Rev. A*, vol. 74, no. 5, p. 051802, 2006.

[5] S. L. McCall, A. F. J. Levi, R. E. Slusher, S. J. Pearton, and R. A. Logan, "Whispering-gallery mode microdisk lasers," *Appl. Phys. Lett.*, vol. 60, no. 3, pp. 289–291, 1992.

[6] A. Polman, B. Min, J. Kalkman, T. J. Kippenberg, and K. J. Vahala, "Ultralow-threshold erbium-implanted toroidal microlaser on silicon," *Appl. Phys. Lett.*, vol. 84, no. 7, pp. 1037–1039, 2004.

[7] P. DelHáye, A. Schliesser, O. Arcizet, T. Wilken, R. Holzwarth, and T. J. Kippenberg, "Optical frequency comb generation from a monolithic microresonator," *Nature*, vol. 450, no. 7173, pp. 1214–1217, 2007.

[8] M. Ferrera, D. Duchesne, L. Razzari, M. Peccianti, R. Morandotti, P. Cheben, S. Janz, D.-X. Xu, B. E. Little, S. Chu, and D. J. Moss, "Low power four wave mixing in an integrated, micro-ring resonator with $Q = 1.2$ million," *Opt. Exp.*, vol. 17, no. 16, pp. 14 098–14 103, 2009.

[9] K. Srinivasan and O. Painter, "Linear and nonlinear optical spectroscopy of a strongly coupled microdisk-quantum dot system," *Nature*, vol. 450, no. 7171, pp. 862–865, 2007.

[10] K. Srinivasan, M. Borselli, O. Painter, A. Stintz, and S. Krishna, "Cavity Q, mode volume, and lasing threshold in small diameter AlGaAs microdisks with embedded quantum dots," *Opt. Exp.*, vol. 14, no. 3, pp. 1094–1105, 2006.

[11] R. D. Kekatpure and M. L. Brongersma, "Quantification of free-carrier absorption in silicon nanocrystals with an optical microcavity," *Nano Lett.*, vol. 8, no. 11, p. 3787, 2008.

[12] R. D. Kekatpure and M. L. Brongersma, "Fundamental photophysics and optical loss processes in Si-nanocrystal-doped microdisk resonators," *Phys. Rev. A*, vol. 78, no. 2, p. 023829, 2008.

[13] S. M. Spillane, T. J. Kippenberg, K. J. Vahala, K. W. Goh, E. Wilcut, and H. J. Kimble, "Ultrahigh-Q toroidal microresonators for cavity quantum electrodynamics," *Phys. Rev. A*, vol. 71, no. 1, p. 013817, 2005.

[14] S. M. Spillane, T. J. Kippenberg, and K. J. Vahala, "Ultralow-threshold Raman laser using a spherical dielectric microcavity," *Nature*, vol. 415, no. 6872, pp. 621–623, 2002.

[15] P. T. Rakich, M. A. Popovic, M. Soljacic, and E. P. Ippen, "Trapping, corralling and spectral bonding of optical resonances through optically induced potentials," *Nat. Photon.*, vol. 1, no. 11, pp. 658–665, Nov. 2007, 11.

[16] Photon Design, Fimmwave [Online]. Available: http://www.photond.com/products/fimmwave.htm

[17] (2007) Rsoft Design Group, Femsim [Online]. Available: http://www.rsoftdesign.com

[18] W. Lui, C.-L. Xu, T. Hirono, K. Yokoyama, and W.-P. Huang, "Full-vectorial wave propagation in semiconductor optical bending waveguides and equivalent straight waveguide approximations," *J. Lightw. Technol.*, vol. 16, no. 5, pp. 910–914, May 1998.

[19] N.-N. Feng, G.-R. Zhou, C. Xu, and W.-P. Huang, "Computation of full-vector modes for bending waveguide using cylindrical perfectly matched layers," *J. Lightw. Technol.*, vol. 20, no. 11, pp. 1976–1980, Nov. 2002.

[20] J. Xiao, H. Ni, and X. Sun, "Full-vector mode solver for bending waveguides based on the finite-difference frequency-domain method in cylindrical coordinate systems," *Opt. Lett.*, vol. 33, no. 16, pp. 1848–1850, 2008.

[21] M. Popovic, "Theory and design of high-index-contrast microphotonic circuits," Ph.D. dissertation, Massachusetts Institute of Technology, Cambridge, 2008.

[22] W. C. Chew, "Electromagnetic theory on a lattice," *J. Appl. Phys.*, vol. 75, no. 10, pp. 4843–4850, 1994.

[23] S. F. Preble, Q. Xu, and M. Lipson, "Changing the colour of light in a silicon resonator," *Nature Photon.*, vol. 1, no. 5, pp. 293–296, 2007.

[24] F. Teixeira and W. Chew, "PML-FDTD in cylindrical and spherical grids," *IEEE Microw. Guided Wave Lett.*, vol. 7, no. 9, pp. 285–287, 1997.

[25] F. Teixeira and W. Chew, "Systematic derivation of anisotropic PML absorbing media in cylindrical and spherical coordinates," *IEEE Microw. Guided Wave Lett.*, vol. 7, no. 11, pp. 371–373, 1997.

[26] B. Little, J.-P. Laine, and H. Haus, "Analytic theory of coupling from tapered fibers and half-blocks into microsphere resonators," *J. Lightw. Technol.*, vol. 17, no. 4, pp. 704–715, 1999.

[27] J. Jin, *The Finite Element Method in Electromagnetics*, 2nd ed. New York: Wiley, 2002.

[28] (2007) Comsol Multiphysics v. 3.3a [Online]. Available: http://www.comsol.com

[29] M. Oxborrow, "Traceable 2-D finite-element simulation of the whispering-gallery modes of axisymmetric electromagnetic resonators," *IEEE Trans. Microw. Theory Techn.*, vol. 55, no. 6, pp. 1209–1218, 2007.

Rohan D. Kekatpure received the B.Tech. degree from Indian Institute of Technology Bombay, India, in 2002 and the M.S. and Ph.D. degrees from Stanford University, Stanford, CA, in 2004 and 2009, all in electrical engineering.

He is currently a Postdoctoral Scholar in the Applied Photonics and Microsystems Division at Sandia National Laboratories, Albuquerque, NM. His research interests include silicon photonics, plasmonics, metamaterials, and numerical methods and he has published over 25 peer reviewed and conference proceedings in these areas.